Experimental study of high-lying states in ^{28}Mg using the resonant elastic scattering of α particles

J. Walshe,[1,*] M. Freer,[1] C. Wheldon,[1] A. Soylu,[2] N. L. Achouri,[3] N. I. Ashwood,[1] W. N. Catford,[4] I. C. Celik,[4] N. Curtis,[1] F. Delaunay,[5] B. Fernández-Domínguez,[6] L. Grassi,[7] Tz. Kokalova,[1] F. M. Marqués,[5] N. A. Orr,[5] L. Prepolec,[7] V. Scuderi,[8] N. Soić,[7] and V. Tokić[7]

[1]*School of Physics and Astronomy, University of Birmingham, Edgbaston, Birmingham B15 2TT, United Kingdom*
[2]*Department of Physics, Nigde University, 51240, Nigde, Turkey*
[3]*Laboratoire de Physique Corpusculaire de Caen, 6 Boulevard Maréchal Juin, 14050 Caen Cedex, France*
[4]*Department of Physics, University of Surrey, Guildford, Surrey, GU2 7XH, United Kingdom*
[5]*Laboratoire de Physique Corpusculaire de Caen, 6 Boulevard Maréchal Juin, 14050 Caen Cedex, France*
[6]*Universidade de Santiago de Compostela, Praza do Obradoiro, 15782 Santiago de Compostela, Spain*
[7]*Institut Ruer Bošković, Bijenička cesta 54, 10000 Zagreb, Croatia*
[8]*INFN - Laboratori Nazionali del Sud, via S.Sofia 62, 95125 Catania, Italy*

(Received 15 August 2016; published 4 November 2016)

The excitation function of ^{28}Mg above the α-decay threshold has been measured for the first time using the resonant scattering of α particles with the technique of a thick target in inverse kinematics. Thirteen new states are reported between $E_x = 15.5$ and $E_x = 20.5$ MeV, and suggestions for spin-parity assignments are given for two of these. Calculations of the branching ratio to α decay for these states as well as comparison of the measured cross sections to calculations suggest that $\alpha + {}^{24}\mathrm{Ne}_{\mathrm{g.s.}}$ clustering is not dominant in this energy regime.

DOI: 10.1103/PhysRevC.94.054304

I. INTRODUCTION

The concept of α clustering is well established in $N = Z$ light nuclei [1,2], and there is increasing evidence for this phenomenon in neutron-rich nuclei. The most well known case is that of the neutron-rich beryllium isotopes: Seya *et al.* [3] showed that the binding energies of $^{8-14}$Be are well reproduced by a model that is based on α-α cluster structure, and more recent antisymmetrized molecular dynamics (AMD) calculations (a method thoroughly reviewed in Ref. [4]) have shown that this cluster structure emerges from an *ab initio* approach where there are no *a priori* assumptions about clustering [5]. The AMD calculations allow inspection of the single-particle wave functions of the valence neutrons, which are found to resemble those of atomic molecular orbitals. In particular, neutrons in σ orbitals—associated with localization of the neutron probability density along the axis joining the α cores—are seen to enhance the cluster structure. Conversely, π orbitals, where the bond axis is perpendicular to the symmetry axes of the component orbitals, are seen to reduce it. The same calculations reproduce observed binding energies and nuclear radii well, supporting this interpretation.

A similar pattern of experimental data is beginning to emerge for the neon isotopes. The picture of ^{20}Ne as a two body α+^{16}O system is supported by the presence of rotational bands the members of which have large reduced widths for α decay [6], and the concept of molecular orbitals for valence neutrons has been extended to ^{21}Ne [7,8]. In a study of ^{22}Ne [9], a strongly α-decaying rotational band is again identified where neutrons are exchanged between the ^{16}O and α cores. AMD calculations [10] also suggested the presence of molecular orbital bands where the cluster structure is again enhanced by two valence neutrons in σ orbitals, although these states were not associated with those in the experimental study.

Given the evidence for α clustering in the neon isotopes, it is reasonable to suggest that this phenomenon may also be present in the analogous symmetric magnesium nuclei. Such structures would be of the form $\alpha + xn + {}^{16}\mathrm{O} + xn + \alpha$, and would represent the most complex nuclear molecules yet observed. This idea is proposed and illustrated by von Oertzen [7] with an extended Ikeda diagram. Of particular interest is the ^{28}Mg nucleus, which is labeled *nuclear water* because of the similarity of the He_2O structure to that of the H_2O molecule [7].

Previous studies of ^{28}Mg have used either the two-neutron transfer reaction $^{26}\mathrm{Mg}(t,p)$ [11–14] or the β decay of ^{28}Na [15–17]. These works have resulted in the measurement and characterization of levels up to an excitation energy of 8.4 MeV [18]. The current work reports results using the resonant elastic scattering of α particles with ^{24}Ne, thus directly populating ^{28}Mg above the threshold for α decay, which occurs at 11.5 MeV—an entirely uncharted energy region for this nucleus.

II. EXPERIMENTAL METHOD

The investigation was performed using the thick target in inverse kinematics (TTIK) technique [19,20]; a schematic of the setup is shown in Fig. 1. A primary beam of ^{26}Mg at 82 MeV/nucleon provided by the cyclotron facility at the Grand Accelerateur National d'Ions Lourds (GANIL) was incident on the carbon production target of the Système de Production d'Ions Radioactifs Accélerateuérés en Ligne (SPIRAL) facility [21,22]. The resulting ^{24}Ne ions were post-accelerated to 3.8 MeV/nucleon by the Cyclotron for Medium Energy Ions (CIME) and collided with a 36-cm-thick helium gas target. The α particles from these reactions were detected using an array of silicon strip detectors placed within the gas.

*Corresponding author: joe.walshe@anu.edu.au

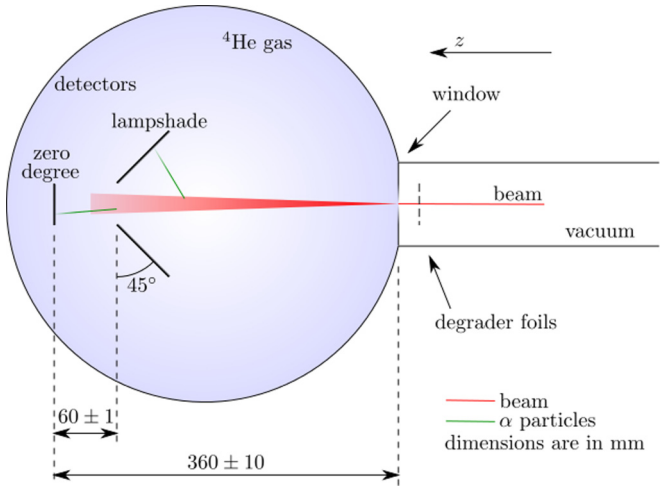

FIG. 1. Schematic of the experimental chamber.

The helium gas served as both the target and energy-loss medium, causing reactions to take place over a continuous range of energies, with the pressure chosen such that the beam was fully stopped within the gas volume. This allowed a detector to be placed at 0° (180° in the center-of-mass (c.m.) frame of the reaction), where the Rutherford cross section is minimum and the resonance scattering cross section is maximum.

The chamber was filled with helium gas to a pressure of 720 mbar, and separated from the beamline by a 4.9 ± 0.5-μm-thick Havar window. The detector at 0° was a 50-mm-square double-sided silicon strip detector, 1000 μm thick, with orthogonal sets of 16 strips on the front and back faces giving an effectively pixelated detector. Away from 0°, a "lamp-shade" array of six single-sided wedge-shaped silicon detectors (Micron YY1 design [23]) was used, with each detector having an active area 80 mm in length from the innermost to the outermost strip. With the beam incident along the z axis, the array provided full azimuthal coverage, and 7°–22° coverage in the polar angle θ, measured in the laboratory frame with the coordinate origin placed at the entrance window. Each of the 16 strips of the wedge detectors represented an approximately constant θ.

Calibration was performed using a ^{239}Pu-^{241}Am-^{244}Cm triple-α source, and because no data currently exist in this excitation energy region for the purposes of comparison, a cross-check was provided by a test beam of ^{20}Ne at 3.5 MeV/nucleon allowing measurement of states in ^{24}Mg for which a significant amount of experimental data are available. Three additional Havar degraders were available upstream of the window in order to provide different beam energies for the purposes of identifying inelastic events. Changing the foil thickness by 2 μm allowed stepping of the beam energy by approximately 10 MeV and thus the c.m. energy by approximately 1.5 MeV; the first excited state in ^{24}Ne lies at 2.0 MeV so events that are within 2.0 MeV of the

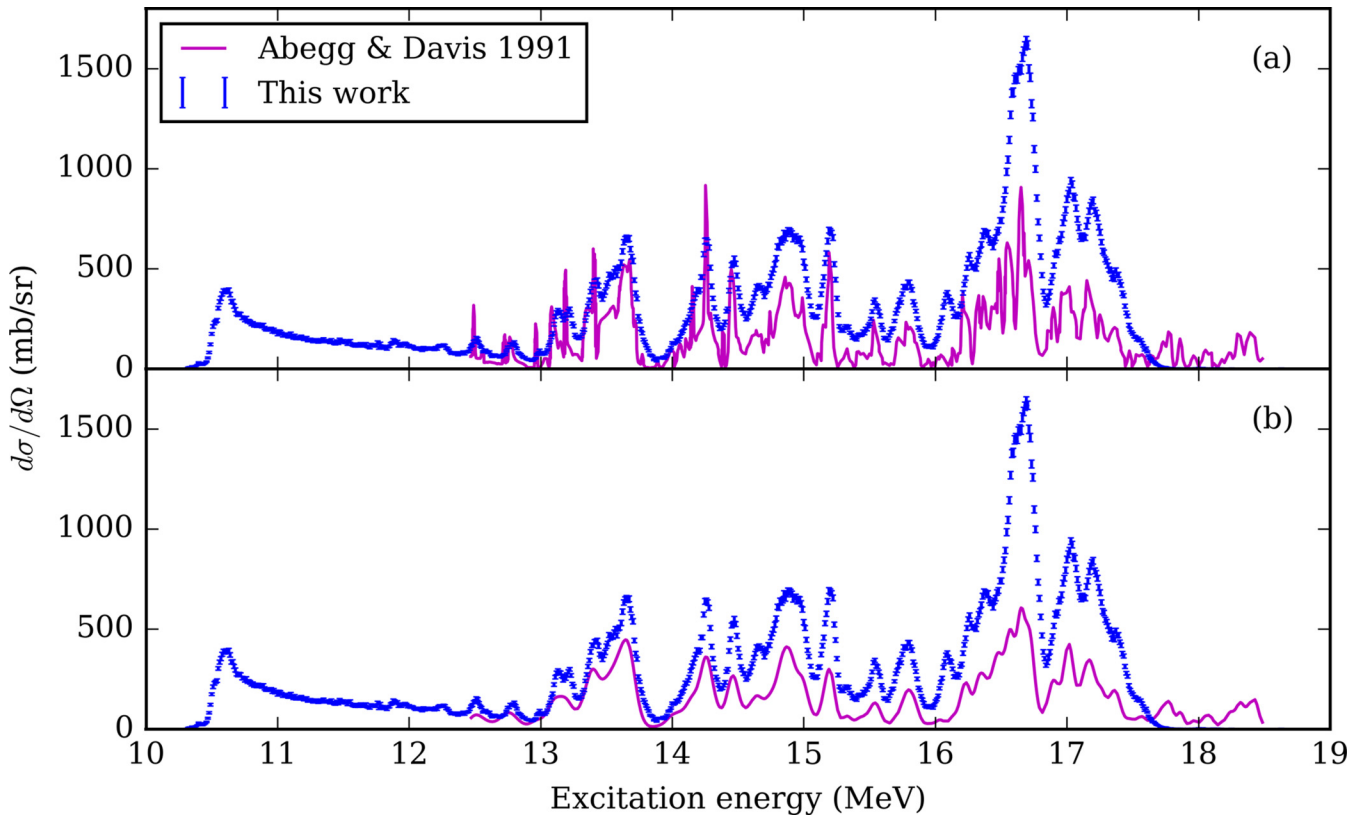

FIG. 2. Comparison of the excitation function of ^{24}Mg measured in this work at 180° and of Ref. [25] measured at 168°. The latter is shown (a) unaltered and (b) after convolution with a resolution of 60 keV FWHM.

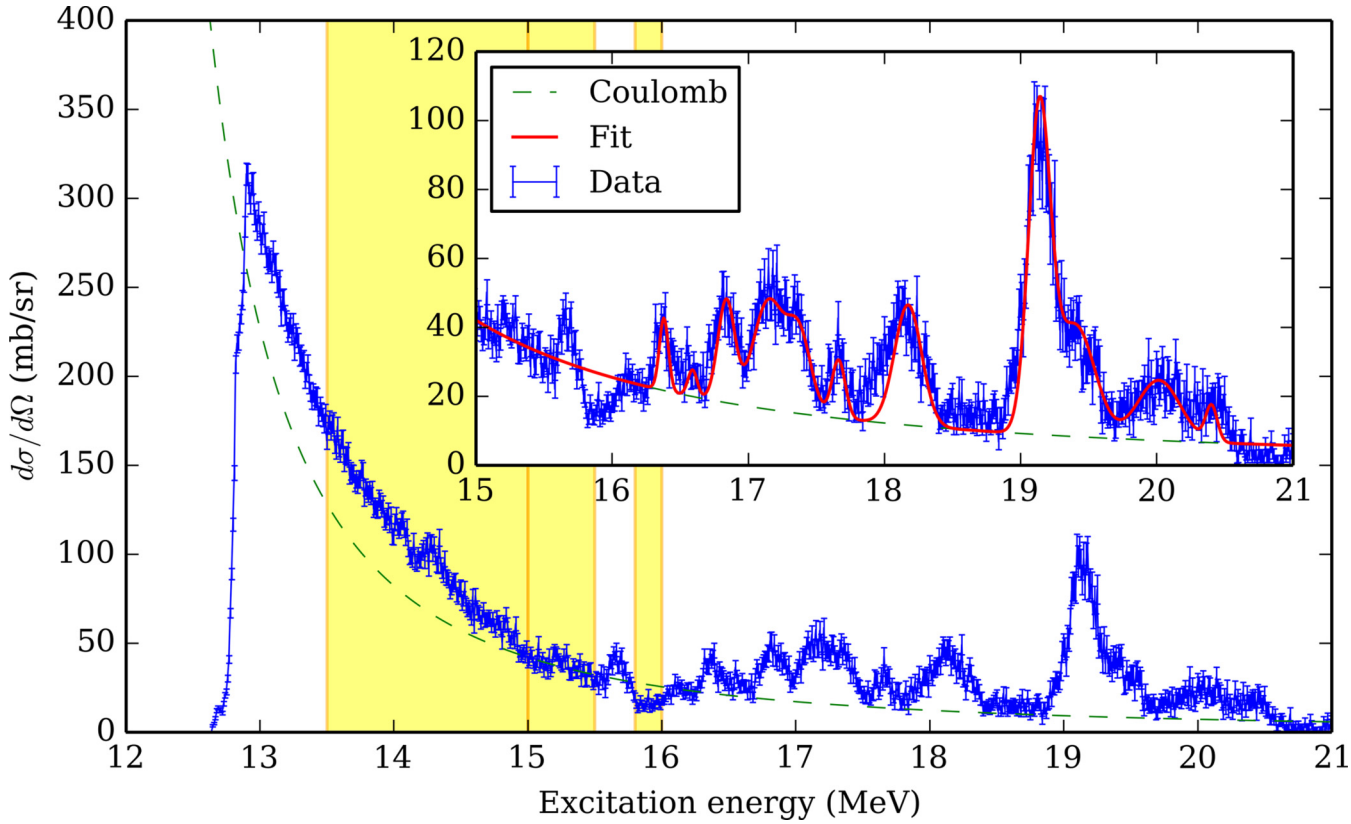

FIG. 3. Excitation energy in ^{28}Mg, showing the calculated Rutherford cross section (green dashed line) that has been used for normalization. The inset shows detail of the resonances with a fit using overlaid Gaussian peak shapes (red solid line). The three regions that were used for normalization of the data are indicated with yellow shading. See text for details.

maximum available excitation energy must result from elastic scattering.

To aid the analysis of the data, an in-house Monte Carlo simulation was used to characterize the performance of the experimental setup. The code REX [24] simulates scattering events that occur according to a chosen excitation function; the beam and the scattered nuclei are tracked through the gas according to calculations of energy loss and straggling effects. The output of the code is a list of detected events that can be analyzed in the same way as the experimental data thus allowing characterization of the resolution and efficiency of the experiment. In addition, each smearing effect can be included or excluded individually, allowing the contribution to the resolution of each to be determined. REX is described in full in Ref. [24].

III. RESULTS

The energies of events in the zero-degree detector were transformed into the c.m. frame using an inverse kinematics calculation, which also took into account the energy loss in the gas. Since particle identification was not available, it was assumed that all detected particles were α particles. Since, in the measured energy range, the only open decay channels are neutron, α, and proton (see Table II), and the proton channel can be expected to be strongly inhibited by the Coulomb barrier, interpreting all events as α particles is a valid assumption. By assuming that the detected α particles have been elastically scattered, the reaction c.m. energy can be unambiguously reconstructed. In addition, each c.m. energy corresponds to a certain depth in the gas, allowing the data to be corrected for the geometrical efficiency of the detector array which varies with the distance of the events from the array. This correction was applied using a REX simulation which calculated the efficiency of the detector array as a function of excitation energy in the compound nucleus. The intrinsic energy resolution of the silicon detectors and associated electronics was ~100 keV, which translates to a resolution of ~60 keV FWHM in the c.m. frame.

A. ^{24}Mg

The excitation spectrum obtained for ^{24}Mg is shown in Fig. 2. Relative normalization of the cross section is provided by correcting for efficiency; absolute normalization is then given by comparison to the calculated Rutherford cross section. To check the validity of the method, it can be compared to the data of Abegg and Davis [25] where the same excitation function is measured using a normal kinematics thin-target reaction. That experiment could not measure the cross section at 180°, so the closest angle available (168°) is used. The two spectra are produced for comparison entirely independently: no matching of energies or cross sections has been performed. The data of Ref. [25] are shown both in raw form (top panel),

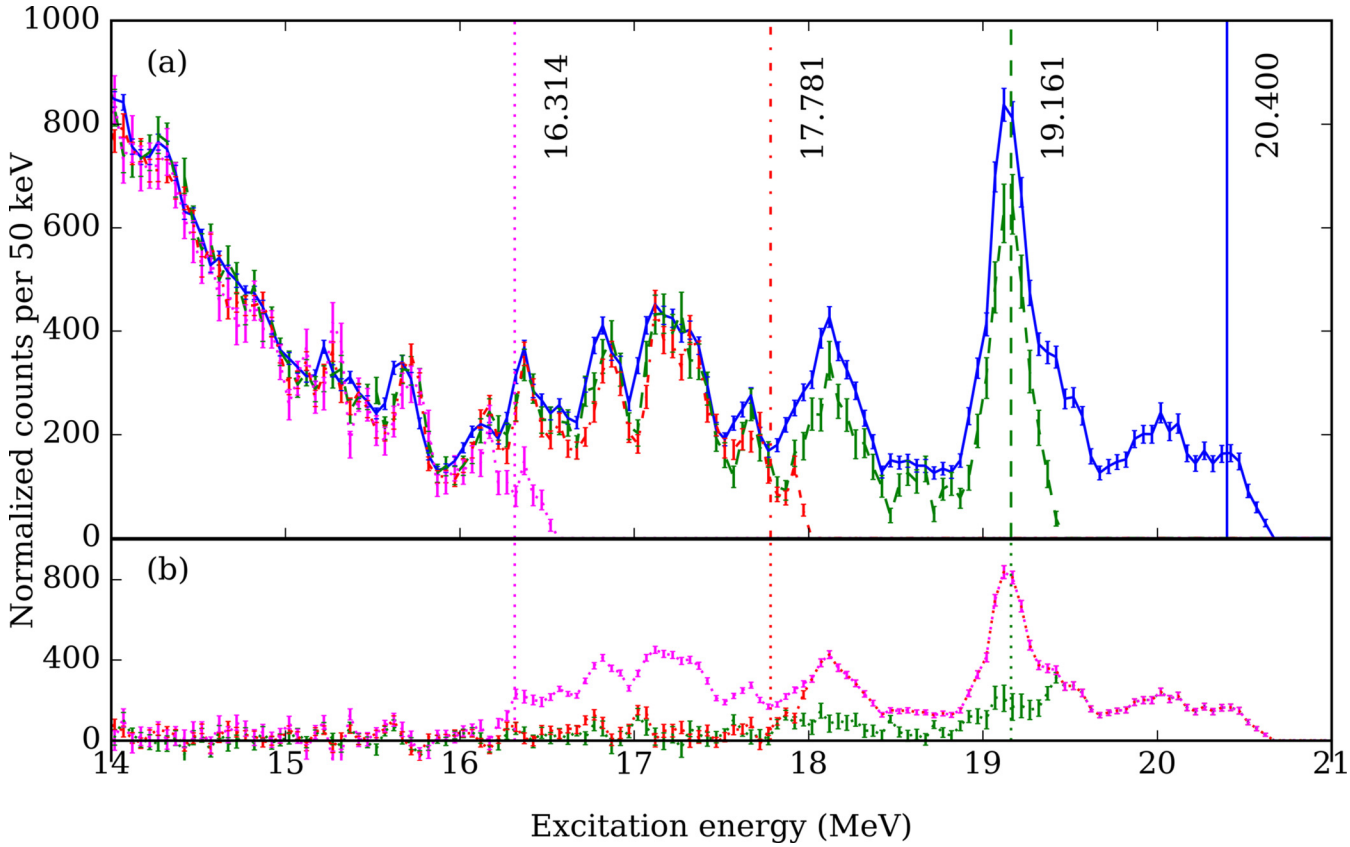

FIG. 4. Comparison of excitation functions for ^{28}Mg measured with four different beam energies, showing (a) the spectra normalized to each other using the Rutherford cross section between 13.1 and 14.0 MeV and (b) the differences between each of the lower beam energy spectra (green with dashed line, red with dot-dashed line, magenta with dotted line) and the spectrum with the highest beam energy (blue with solid line). For each spectrum, the highest available excitation energy is marked.

where the resolution of the thin-target technique is seen to be better than the current work (as it depends primarily on the energy spread of the beam from the tandem accelerator, which is small), and after convolution with a constant resolution of 60 keV FWHM (the approximate energy resolution of the current work). The energy agreement is excellent, and the shapes of both data sets after convolution match very well. Differences in cross section are attributed to the different measurement angles, and larger differences are seen at higher energies as higher spin states (with more sharply peaking angular distributions) become accessible.

The comparison reveals that the experimental detail of the TTIK approach is well understood and that, despite the lack of previous data for comparison, the results for ^{24}Ne+α scattering are also reliable.

B. ^{28}Mg

The resulting excitation energy spectrum for ^{28}Mg is shown in Fig. 3. Also shown is the calculated Rutherford cross section for this reaction, which again provides overall normalization using the region from 15.0 to 15.5 MeV in excitation energy.

Data taken using lower beam energies are shown in Fig. 4 and indicate that there are no significant inelastic contaminants in the spectrum. In total, four different degrader combinations were used giving beam energies entering the gas of 62.6, 53.5, 44.0, and 33.7 MeV. The corresponding excitation energies are marked in Fig. 4. Also shown are the differences between each of the three lower beam energies compared to the highest, demonstrating that there are no significant deviations from zero.

Thirteen new states are identified in the data of Fig. 3, and the energies and widths were found using a fit of Gaussian peak shapes. The fit is shown in Fig. 3, and Table I shows the fitted parameters. The relative strength (area) of each state is also given in arbitrary units relative to the largest state at 19.14 MeV, which is assigned strength = 1. The main contribution to the uncertainty on the fitted parameters is the normalization to the Rutherford cross section, and so this uncertainty was quantified by repeating the fit with the normalization performed using different parts of the spectrum: 13.5–15.0 MeV, 15.0–15.5 MeV, and 15.8–16.0 MeV. These regions are highlighted in Fig. 3. The parameters in Table I are the means of the parameters from each fit; the uncertainties are the standard deviations. If the uncertainty was larger than the result, an upper limit is given. For those states that could not be fit in all cases due to the level of the background, either no uncertainty is given or the result is left blank. It should be noted that the Gaussian fit does not fully reproduce the shape of the 18.14 MeV state. This could be an indication that there is more than one state in this region that cannot be resolved in

TABLE I. Fitted parameters for states in ^{28}Mg using Gaussian peak shapes with a Rutherford background. Relative strength gives the area of each state as a fraction of the 19.14 MeV state. Uncertainties are characterized by the variation over three fits; see text for details.

Energy (MeV)	FWHM (keV)	Area (mb/sr)	Relative strength
15.664(5)	70(60)		<0.2
16.1	100		<0.1
16.377(7)	120(80)		<0.3
16.55(5)	120(40)	150(130)	0.06(5)
16.836(5)	190(50)	790(590)	0.30(23)
17.13(2)	220(40)	870(280)	0.33(11)
17.35(3)	230(30)	910(660)	0.35(25)
17.656(8)	130(30)	330(230)	0.12(9)
18.14(3)	340(100)	1500(1000)	0.59(40)
19.144(4)	230(60)	2600(1400)	1.00(52)
19.43(4)	280(70)	1070(380)	0.41(15)
20.04(2)	350(40)	920(520)	0.35(20)
20.414(8)	90(10)	170(110)	0.07(4)

this experiment; however, since there is no clear indicator for multiple states only one was included in the fit.

The data from the entire silicon array are shown in Fig. 5 where the energy of each event is plotted against angle in the laboratory frame relative to the entrance window of the chamber. The experimental resolution becomes worse for low energies (i.e., scattering events that are closer to the detectors) and large scattering angles. Calculation of the scattering angle is performed after choosing a random position for each event within the strip or pixel where it is detected, in order to improve the legibility of figures.

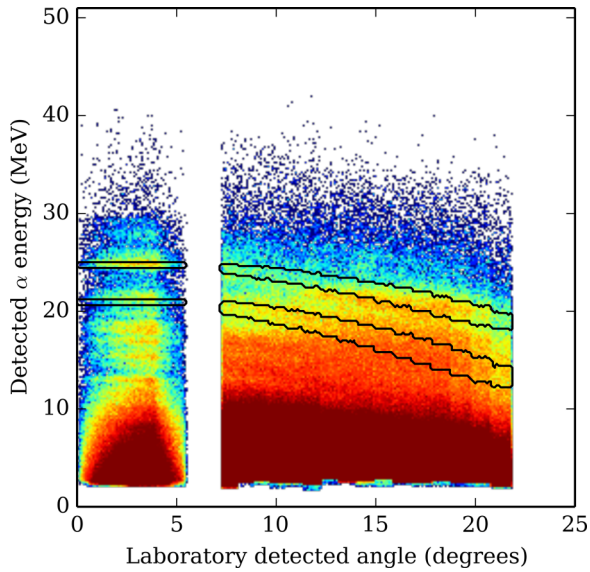

FIG. 5. Energy of all α particles from ^{28}Mg plotted against angle, measured with the coordinate origin placed at the entrance window. The data in the left-hand block are from the zero-degree detector, and those in the right-hand block are from the lamp-shade array. The software gates used to obtain angular distributions are shown; see text for details of the gating procedure.

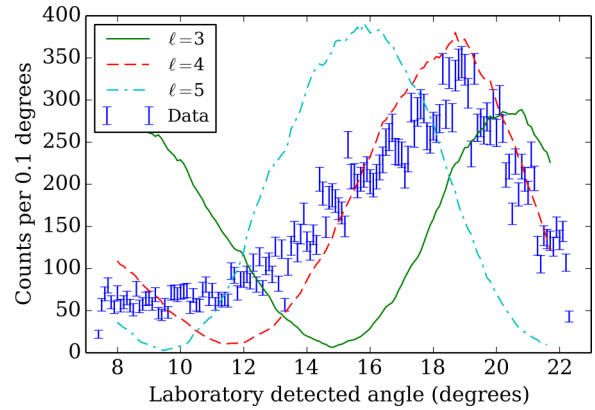

FIG. 6. Angular distribution for the state at 19.14 MeV (points with error bars), with simulated distributions (lines).

The angular distributions were obtained by drawing a software gate around the relevant portion of events in Fig. 5 and using these data to create a spectrum for the angular distributions. REX simulations of a state at the excitation energy of interest, with a uniform angular distribution, were used to deduce the position of the gates in Fig. 5 as this method shows the loci of the kinematic lines for each state in the laboratory frame. The simulations also give the experimental resolution and so the spread of the angular distribution.

REX was also used to deduce the spin of each state by simulating the angular distributions of states at the relevant energies for a known series of spins in order to compare to the data. In the c.m. frame, the angular distributions are given by Legendre polynomials of order ℓ, where ℓ corresponds to the spin of the state. In the laboratory frame, the locations of the maxima and minima also depend on the excitation energy of the state; the distributions are further modulated by the array efficiency which is a function of both energy and scattering angle. These effects are discussed in detail in Ref. [24]. The data are then compared to the simulated distributions to find the spins of the states.

Fig. 6 shows the angular distribution for the state at 19.14 MeV, along with a selection of the simulated distributions. A bin size of 0.1° has been chosen for clarity, though it should be noted that the angular resolution is not this high. The data show strong agreement with the $\ell = 4$ case due to the matching positions of the maxima. A state of a lower spin than those shown would not give as large a variation in count rate across the measured region, while a larger spin would be evidenced by the presence of multiple maxima. The absence of a minimum matching the simulated distributions indicates there may be other, minor, contributions to the spectrum, which distort the angular distributions.

The distribution from the second gate, corresponding to the state at 18.14 MeV, is shown in Fig. 7. Simulations are again shown, but in this case the agreement is not as clear as for the 19.14 MeV state. The energy width of the gate was varied and the resulting distributions compared to show which components are strongest at the center: a wide gate gave an angular distribution that was consistent with $\ell = 0$, most likely due to the mixing of distributions from multiple states. As the

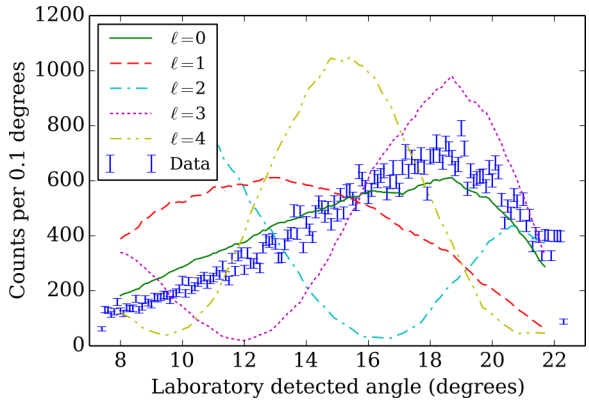

FIG. 7. Angular distribution for the state at 18.14 MeV (points with error bars), with simulated distributions (lines).

gate is narrowed, a maximum starts to appear that is most consistent with $\ell = 3$, and this narrow gate is shown in Fig. 7. The nature of the angular distribution as well as the quality of the Gaussian fit in this region suggest that there may be more than one state within the measured peak.

IV. DISCUSSION

While only the α channel has been measured, the spin determination described above allows an estimate to be made of the partial α width, $\Gamma_\alpha/\Gamma_{\rm tot}$, as the measured cross section in the α channel depends on both the partial and total widths. Table II lists the decay channels that were open in this experiment. Since the threshold for proton decay is high (16.8 MeV), with the available energy proton decay will be strongly suppressed by the Coulomb barrier. The R-matrix penetrability for a proton-decaying $\ell = 4$ state at 19.14 MeV is $P_\ell = 10^{-3}$, compared to $P_\ell = 2.5$ for the α channel. Since strong contributions from inelastic channels are not present, as discussed in Sec. III B, it is reasonable to expect that the only other competing channel in the measured energy range is neutron decay.

For the state at 19.14 MeV, an R-matrix calculation was performed using the code AZURE2 [26], with input parameters being the measured level energy and spin from the above analysis. The code performed a fit, varying the widths in the α and neutron channels only, in order to obtain a value for the branching ratio for α decay. The resulting fit is shown in Fig. 8, and the fitted widths are given in Table III.

Using the measurement of Γ_α and $\Gamma_{\rm tot}$, an initial indicator of the extent of clustering can be made by calculating the reduced width for α decay, γ_α^2, and comparing this value to the Wigner

TABLE II. Decay thresholds for ^{28}Mg [18].

Decay channel	Threshold energy (MeV)
n	8.505
α	11.492
$2n$	14.947
p	16.790

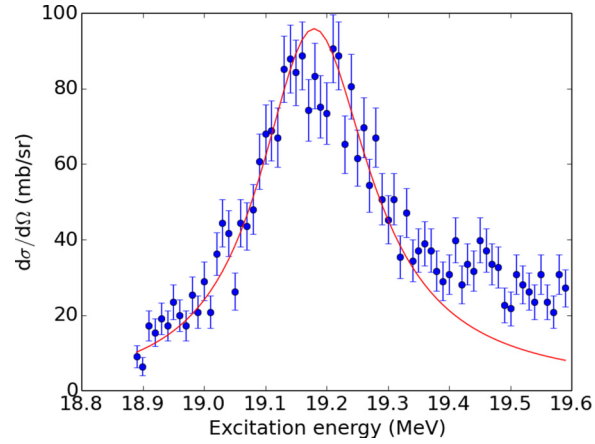

FIG. 8. R-matrix fit (red line) to the state (blue circles) at 19.14 MeV with $J^\pi = 4^+$. A clear shoulder on the high energy side of the peak has been ignored in the fit. In the fitting region ($E_x = 18.9$–19.3 MeV) $\chi^2/\text{d.o.f} = 1.22$.

limit, γ_W^2, given by

$$\gamma_W^2 = \frac{3\hbar^2}{2\mu R_c^2}, \tag{1}$$

with the channel radius R_c. This was calculated using the mass numbers of the interacting nuclei, $A_{\rm Ne}$ and A_α, from

$$R_c = r_0\left(A_{\rm Ne}^{1/3} + A_\alpha^{1/3}\right), \tag{2}$$

where $r_0 = 1.4$ fm. These calculations were performed using an in-house code, CKIN [27], which includes the routine WCLBES from the CERN libraries [28]. For the state at 19.14 MeV, with $J^\pi = 4^+$ and $\Gamma_\alpha/\Gamma_{\rm tot} = 0.38$, this gave a value of $\gamma_\alpha^2/\gamma_W^2 = 3.8\%$, suggesting that α clustering is suppressed.

Assuming that the only decay mode of the state other than α decay is via the single neutron channel, i.e., $\Gamma_n = \Gamma_{\rm tot} - \Gamma_\alpha$, a value of $\Gamma_n = 150$ keV would be found, which represents an upper limit for the neutron decay width from this state. The code GAMOW [29] was used to calculate the neutron decay width by solving the Schrödinger equation for a neutron in the potential produced by the ^{27}Mg nucleus. The potential used in the calculations was a standard Woods-Saxon shape, given by

$$V(r) = -V_0\frac{1}{1+e^{(r-R)/a}}, \tag{3}$$

where R is the radius parameter, with $R = r_0 A_T^{1/3}$ and $A_T = 27$, and a is the diffuseness parameter. An initial value of $V_0 = 100$ MeV was used. Using $r_0 = 1.4$ fm and $a = 0.5$ fm gives $\Gamma_n = 5.1$ MeV, much greater than the measured value,

TABLE III. Level widths in ^{28}Mg from R-matrix fitting.

State energy (MeV)	J^π	Γ_α (keV)	$\Gamma_{\rm tot}$ (keV)	$\Gamma_\alpha/\Gamma_{\rm tot}$	γ_α/γ_W (%)
19.14	4^+	90	240	0.38	3.8
18.14	(3^-)	140	340	0.29	6.0

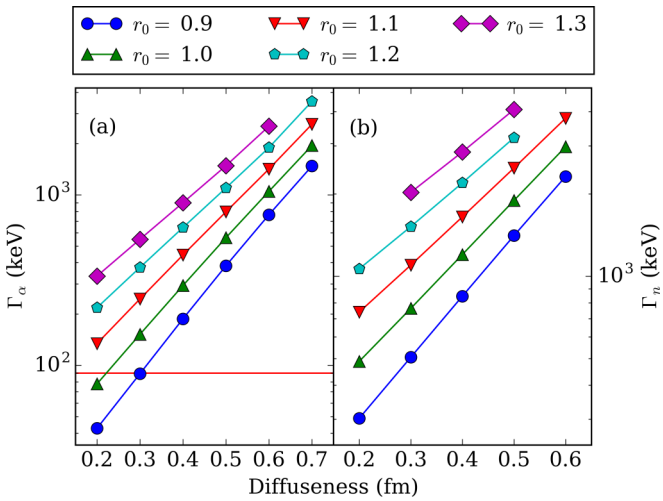

FIG. 9. Calculated widths for the α and neutron channels, (a) Γ_α and (b) Γ_n, using the code GAMOW, as a function of the radius and diffuseness parameters r_0 and a. A horizontal red line shows the experimental value of Γ_α (90 keV); the corresponding value for Γ_n found using an R-matrix calculation (150 keV) is not visible on this scale.

suggesting that this state is much longer lived than may be expected from this simple model. Reproducing the measured width with this potential requires much smaller parameters which do not have any physical meaning.

The GAMOW code can also be used to calculate the decay width that would be expected for an α particle interacting with a ^{24}Ne core, i.e., for an α-clustered state. The results of these calculations for both Γ_α and Γ_n are summarized in Fig. 9, which shows that in order to reproduce the experimental widths, unusually small values of r_0 and a are required. This suggests that the measured states are not α clustered.

The R-matrix fitting analysis was repeated for the state at 18.14 MeV, assuming a spin-parity of $J^\pi = 3^-$, and the results are included in Table III. Again, the results suggest that α clustering is not prominent. In addition, an R-matrix calculation of a state at this energy with $J^\pi = 0^+$ cannot reproduce the experimental cross section even with $\Gamma_\alpha = \Gamma_{\text{tot}}$, supporting the conclusion that this feature is not the result of a single 0^+ state.

While analysis of the branching ratio to α decay is only possible for the two states with spin-parity assignments, it is clear that if there were any strongly α-clustered states within the measured energy region they would have been identified with this experimental method. This measurement suggests, therefore, that α clustering is not dominant anywhere in this energy range. It is of interest to note that the thresholds for the ^{23}Ne+n+α and ^{22}Ne+2n+α structures lie at 20.4 and 25.6 MeV, respectively, and therefore molecular structures would be expected to be enhanced at or above these energies. Hence, the structure of these states remains an open question. A natural extension of this work would be to extend the measurement of the cross section to higher energies, though it should be noted that many other reaction channels would be opened and therefore the analysis of the data would be more complex.

V. CONCLUSIONS

Thirteen states in ^{28}Mg have been newly identified and the widths for ten of these have been measured. For one of these, at 19.14 MeV, a clear spin assignment of $J^\pi = 4^+$ is given and for a second, at 18.14 MeV, a tentative assignment of $J^\pi = 3^-$ is made. For the state at 19.14 MeV, an R-matrix fit is used to calculate the partial α width and thus the ratio of reduced width to the Wigner limit is found to be 3.8%, which suggests this is not a strongly clustered state. Calculation of the expected neutron width, however, gives a much larger value than is measured, so the nature of this state is not yet clear. More sophisticated calculations are required in order to explain the observed parameters.

In the case of future experimental work aimed at understanding the molecular structure of ^{28}Mg it would be beneficial to increase the size of the measured energy range to include the ^{23}Ne+n+α and ^{22}Ne+2n+α thresholds, which lie at 20.4 and 25.6 MeV, respectively. Observation of the behavior of the cross section as these channels become available would be an indicator of the role of molecular structures in the ^{28}Mg system.

ACKNOWLEDGMENTS

The authors thank the technical staff at GANIL for their assistance during the experiment. We acknowledge the financial support of the UK Science and Technology Facilities Council (STFC), and support from the EC through ENSAR. Tz.K is grateful for a Daphne Jackson grant funded by the STFC.

[1] M. Freer, Rep. Prog. Phys. **70**, 2149 (2007).
[2] W. von Oertzen, M. Freer, and Y. Kanada-En'yo, Phys. Rep. **432**, 43 (2006).
[3] M. Seya, M. Kohno, and S. Nagata, Prog. Theor. Phys. **65**, 204 (1981).
[4] Y. Kanada-En'yo and H. Horiuchi, Prog. Theor. Phys. Suppl. **142**, 205 (2001).
[5] Y. Kanada-En'yo, M. Kimura, and H. Horiuchi, C. R. Phys. **4**, 497 (2003).
[6] H. T. Richards, Phys. Rev. C **29**, 276 (1984).
[7] W. von Oertzen, Eur. Phys. J. A **11**, 403 (2001).
[8] C. Wheldon *et al.*, Eur. Phys. J. A **26**, 321 (2005).
[9] G. Rogachev *et al.*, Phys. Rev. C **64**, 051302(R) (2001).
[10] M. Kimura, Phys. Rev. C **75**, 034312 (2007).
[11] B. Rastegar, G. Guillaum, P. Fintz, and A. Gallmann, Nucl. Phys. A **225**, 80 (1974).
[12] T. Fisher, T. Bardin, J. Becker, L. Chase, D. Kohler, R. McDonald, A. Poletti, and J. Pronko, Phys. Rev. C **7** 1878 (1973).

[13] R. Middleton and D. Pullen, Nucl. Phys. **51**, 77 (1964).
[14] S. Hinds, H. Marchant, and R. Middleton, Proc. Phys. Soc. **78**, 473 (1961).
[15] K. Kura *et al.*, Phys. Rev. C **85** 034310 (2012).
[16] D. Guillemaud-Mueller, C. Détraz, M. Langevin, F. Naulin, M. de Saint-Simon, C. Thibault, F. Touchard, and M. Epherre, Nucl. Phys. A **426**, 37 (1984).
[17] C. Détraz, D. Guillemaid, G. Huber, R. Klapisch, M. Langevin, F. Naulin, C. Thibault, L. Carraz, and F. Touchard, Phys. Rev. C **19**, 164 (1979).
[18] National Nuclear Data Center, The Chart of Nuclides, http://www.nndc.bnl.gov/chart/.
[19] K. Artemov *et al.*, Sov. J. Nucl. Phys. **52**, 408 (1990).
[20] J. Walshe *et al.*, J. Phys.: Conf. Ser. **569** 012052 (2014).
[21] C. Detraz, Nature **315**, 291 (1985).
[22] A. Villari, Nucl. Instrum. Methods B **204**, 31 (2003).
[23] T. Davinson *et al.*, Nucl. Instrum. Methods A **454**, 350 (2000).
[24] N. Curtis and J. Walshe, Nucl. Instrum. Methods A **797**, 44 (2015).
[25] R. Abegg and C. A. Davis, Phys. Rev. C **43**, 2523 (1991).
[26] R. Azuma *et al.*, Phys. Rev. C **81** 045805 (2010).
[27] C. Wheldon, CKIN, http://www.wheldon.talktalk.net/files/ckin.c.
[28] CERN program library, https://cernlib.web.cern.ch/cernlib/.
[29] T. Vertse, K. Pal, and Z. Balogh, Comput. Phys. Commun. **27**, 309 (1982).